

Optical characterization of chevron texture formation in nematic electroconvection

H. Amm, R. Stannarius, and A. G. Rossberg[†]

Universität Leipzig, Fak. Physik und Geowiss., Linnéstr. 5, D-04103 Leipzig, Germany

[†]*Universität Bayreuth, Physikalisches Inst. D-95440 Bayreuth, Germany*

(Received November 18, 2018)

Abstract

We characterize the director structures in electroconvection patterns of nematic liquid crystals by means of polarising microscopy. This study was stimulated by a theory put forward by Rossberg et al. [1] who propose a mechanism for chevron texture formation. We characterize the relation between the wave vector modulation and in-plane twist modulations of the director field. In addition to the standard optical setup, a circular analyzer is used. The results provide new insight into the interplay of director and wave vector field leading to the chevron texture and fluctuating conductive rolls. Our experimental results confirm the theoretical predictions.

INTRODUCTION

Electroconvection (EC) in nematics is a well known standard system for dissipative pattern formation. It provides a rich scenario of dissipative structures which can be readily controlled by experimental parameters as electric field strength and frequency. The study of EC in nematics has attracted much interest during the last decades. The hydrodynamic and electric equations involved are well known. Observation of the textures is straightforward by means of optical microscopy. Much progress has been made during the last decades in the theoretical understanding of the pattern selection process. The basic classification and physical mechanism of the different patterns are well understood.

The system has still retained its attractivity for scientific research [2]. Because of its high complexity, many features have found theoretical explanation only recently or still lack sufficient understanding. While the periodicity and orientation of the optical patterns can be easily studied with transmission microscopy, the description of the director field in the convection structures is still not fully revealed. Most experiments with EC so far have been restricted to observations in unpolarized light or in a polarizing microscope with polarizers along the director easy axis \vec{n}_0 . In that geometry, periodical tilt modulations of the director generate a lense effect and produce a periodically modulated transmission texture which maps the director pattern. The optical characteristics can be calculated numerically using Fermat's principle, and a relation between the observed texture and the director tilt profile can be established at least for the simplest convection roll patterns.

One of the more complex patterns that can be observed is the "chevron texture" which is named after a characteristic periodic modulation of the roll orientation as it can be seen in Figs. 6,7. An explanation of the formation of such chevron patterns has been suggested recently [1]. In order to describe the appearance of chevron patterns from a homogeneously defect-chaotic state, the authors propose a set of model equations of the reaction-diffusion type, which is well known to lead to spatially modulated patterns (*Turing*-patterns) under appropriate conditions. The roles of fast and the slowly diffusing species in these model

equations are played by the in-plane director reorientation (in the present case a twist which is superimposed to the usual periodic tilt structure of the convection rolls) and the orientation of the wave vector of the rolls, respectively. While the "diffusion" of the director twist is mediated by the bend elastic forces of the liquid crystal, the wave vector diffuses by the irregular motion of individual defects, which is characteristic for the defect-chaotic state. The theoretical description has been developed originally for systems with weakly broken isotropic symmetry, as represented by EC in homeotropic cells under the influence of a lateral magnetic field. In that case, the proposed mechanism leads to a periodic bend deformation of the director accompanied by a corresponding modulation of the wave vector of the roll patterns. In the system studied here, EC in planar cells, the situation is more complex due to the preferred alignment axis of the director at the glass plates. The director remains fixed at the upper and lower cell boundaries while it twists out of the alignment axis in the cell middle. A twist deformation along the cell normal is expected to arise.

The local director and the wave vector of the rolls interact by a systematic drift of defects which is induced by the director twist and leads to a change of the wave vector. In addition, director and wave vector are coupled by a hydrodynamic torque on the director, which must generally be expected when the director is not aligned perfectly normal to the rolls. For liquid crystal convection this torque seems generally to increase misalignment [3,4]. If the director would play a rather passive roll in chevron formation, one might expect that director and wave vector are deflected in opposite directions. In contrast, according to the proposed model, the linear mode associated with the chevron formation must contain both the well known long-range modulation of the wave vector and a modulated director twist in phase with it. In fact the amplitudes of the two components are expected to be of similar size.

Within this study, we have focused our investigation on the detection of such out-of-plane (out of the tilt plane between surface alignment and cell normal) twist director deflections, in addition to the standard characterization of the dielectric convection structures. With modified optical techniques, we analyse the complex structure of the director field and its relation to the wave vector field of the convection rolls. In standard planar cells with ≈ 20

to $100\mu\text{m}$ cell gap, small director twist cannot be detected in the conventional experiment. The polarization plane of incident light is guided adiabatically with the director twist along the cell normal, and it is rotated back before leaving the nematic layer. This phenomenon known as wave guiding is effective as long as the so called *Mauguin* limit holds [11], that is the optical axis of the anisotropic medium changes its orientation in space sufficiently slowly on the wavelength scale. Therefore, the optical transmission intensity is practically uninfluenced by moderate director twist [12,13]. In conventional experiments, only the tilt profile of the EC patterns is accessed, information on the director field is incomplete. Possible director twist is usually neglected in the description of EC patterns. The actually three-dimensional director field has not been characterized yet because of the experimental limitations.

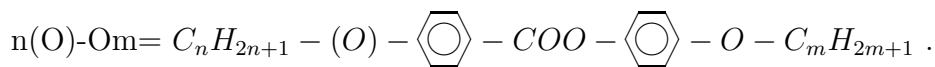
However, it is well known that a small modification of the optical setup, the insertion of a quarterwave plate at 45° orientation to the polarizers raises the degeneracy between clockwise and counterclockwise twisted domains. It can be used to visualize twist deformations in the nematic sample [19]. Using such a phase plate, we record the contrast modulation in the cell plane which is a measure of the director twist pattern. We compare these twist modulations with the arrangement of the convection rolls.

SUBSTANCES AND EXPERIMENTAL SETUP

We use glass cells with transparent ITO electrodes and antiparallel rubbed polyimide layers for rigid planar surface anchoring of the nematic. The nematic liquid crystal was a four component mixture (*Mischung 5*) of alkyloxyphenyl-alkyl(oxy)benzoates

1O-O6: 22.0% 5O-O8: 30.3%

6O-O7: 13.3% 6 -O4: 34.4%.



Its nematic range extends from 70.5°C to below RT. *Mischung 5* is well characterized as a nematic standard substance (e.g. [20,21]). The substance has a small negative dielectric

anisotropy $\epsilon_{\parallel} - \epsilon_{\perp}$. All measurements were performed at 30°C. The refractive indices at 30°C are $n_e = 1.6315$ and $n_o = 1.4935$. These values have also been used in all simulations. Our polarizer-analyzer setup is shown in Fig. 1, two different geometries have been applied. In Fig. 1a, the polarizers are along the rubbing direction such that only the transmission of extraordinary incident light is observed. In this geometry, the convection roll patterns can be studied and information on the director tilt profile is obtained. In the second arrangement shown in Fig. 1b, the polarizer has been rotated perpendicular to the director alignment. Thus, only ordinary incident light is present, and a contrast modulation due to refraction in the periodic tilt profile within the convection rolls is avoided. The quarterwave plate at 45° to the polarizer discriminates domains of right-handed and left-handed director twist. The position of the analyzer can be chosen either parallel or perpendicular to the polarizer, yielding equivalent information (intensities are complementary). The transmission images are recorded with a conventional CCD camera and digitized for numerical processing. It would be desirable in the experiment to take both the tilt and twist sensitive images concurrently, in particular for non-stationary textures. In practice, however, we had to switch polarizer and $\lambda/4$ plate quickly between individual snapshots of the transmission textures. Rapidly fluctuating images (timescale $< 1s$) can therefore be compared only in a qualitative way.

OPTICS

The simulation of the optical characteristics of EC in the standard geometry of Fig. 1a has been extensively studied [5–10]. The optical pattern is generated by diffraction of the incoming extraordinary wave in the periodically modulated refractive index profile of the deformed liquid crystal. The transmission texture of roll cells is a periodic stripe pattern which changes its appearance with the microscopic focus plane. One observes the optical pattern if the incident light is unpolarized or polarized along the director easy axis \vec{n}_0 . The convection roll textures disappear when the incident light is polarized perpendicular to \vec{n}_0 .

Optical transmission of a twisted nematic layer with a phase plate in the geometry of Fig. 1b is influenced by completely different effects. When the polarizers are perpendicular to \vec{n}_0 , we deal with the ordinary incident wave which experiences a constant refractive index independent of director tilt. The texture of a non-twisted but tilt-modulated director field ($n_y = 0$) is uniform. The diffraction effects can be neglected. If the director twists out of the (x, z) tilt plane, the ordinary wave is guided with the twisted director as long as the *Mauguin* condition holds, irrespective of small tilt deformations. The exact analysis shows that the polarization state of incident light is not completely restored. In general the transmitted light is no longer linearly polarized but becomes elliptically polarized. The main axis of the ellipse of the exit beam is rotated out of the incident polarization direction. Due to the symmetry of the system, the rotation is reverse for oppositely twisted domains of the director field, and the effect of the quarterwave plate is contrary.

For a calculation of the optical effects of the director twist, one can apply several approximative methods. A general solution for one-dimensionally deformed nematic layers can be found from the Berreman [15,16] and Jones [17,18] matrix formalism, with and without consideration of internal reflections. Gerber and Schadt have introduced an analytical expression which is valid for small angle twist. Scheffer and Nehring, e.g. have applied a transfer matrix method for the calculation of the optical characteristics of strongly twisted nematic cells [14]. We use this approach and modify the transfer matrix appropriately to describe our experimental observations of the chevron textures. The differences which have to be considered are first that the twist angle is modulated in the cell plane whereas in the twist Fréedericksz transition or in twisted nematic cells, the deformation is uniform in the cell plane, and second we have to take the phase plate into consideration. Finally, there is an additional short-wavelength tilt modulation due to the convection rolls which should affect the extraordinary incident wave, but also the ordinary incident wave at high twist deformations.

The computation of the optical transmission can be performed when some approximations are introduced. We demonstrate for the geometry of Fig. 1b how periodical twist modu-

lations in the sample plane influence the transmission texture. We begin with a director field in the sample which be homogeneous in the (x, y) plane at least on distances large compared to the wavelength, such that plane waves can be assumed. We establish 2×2 optical propagation matrix

$$\bar{P} = \bar{P}_A \times \bar{P}_\lambda \times \bar{P}_{LC} \times \bar{P}_P \quad (1)$$

from the polarizer matrix \bar{P}_P , the propagator matrix in the nematic layer \bar{P}_{LC} , the propagator matrix of the $\lambda/4$ plate \bar{P}_λ , and that of the analyzer \bar{P}_A ,

$$\bar{P}_P = \frac{1}{2} \begin{bmatrix} 1 + \cos 2\alpha_p & \sin 2\alpha_p \\ \sin 2\alpha_p & 1 - \cos 2\alpha_p \end{bmatrix},$$

$$\bar{P}_\lambda = \begin{bmatrix} \cos^2 \alpha_\lambda + i \sin^2 \alpha_\lambda & \sin \alpha_\lambda \cos \alpha_\lambda (1 - i) \\ \sin \alpha_\lambda \cos \alpha_\lambda (1 - i) & \sin^2 \alpha_\lambda + i \cos^2 \alpha_\lambda \end{bmatrix},$$

$$\bar{P}_A = \frac{1}{2} \begin{bmatrix} 1 + \cos 2\alpha_a & \sin 2\alpha_a \\ \sin 2\alpha_a & 1 - \cos 2\alpha_a \end{bmatrix},$$

and $\alpha_p, \alpha_\lambda, \alpha_a$ are the rotation angles of polarizer, phase plate and analyzer with respect to the director easy axis.

The propagation matrix in the nematic layer can be calculated when the nematic is treated as a stratified medium. It is described as a stack of sufficiently thin layers in which the nematic material can be considered homogeneous and the propagation matrix in each slice n is

$$\bar{P}_n = \begin{bmatrix} \exp(2\pi i n_e d_n / \lambda) & 0 \\ 0 & \exp(2\pi i n_o d_n / \lambda) \end{bmatrix}$$

in the local principal axis frame of the director system, with the refractive indices $n_{e,o}$ of the nematic, the vacuum wavelength λ and the thickness d_n of the slices. In the laboratory system it reads

$$\bar{P}_n = \exp(i\psi) \begin{bmatrix} \cos \gamma + i \sin \gamma \cos 2\phi & \sin \gamma \sin 2\phi \\ i \sin \gamma \sin 2\phi & \cos \gamma - i \sin \gamma \cos 2\phi \end{bmatrix}$$

for a slice with the director in the angle ϕ respective to the x axis, with $\gamma = \pi(n_e - n_o)d_n/\lambda$, and $\psi = \pi(n_e + n_o)d_n/\lambda$. The total propagator \bar{P}_{LC} is the product

$$\bar{P}_{LC} = \prod_{n=1}^N \bar{P}_n$$

of the matrices of the individual layers. This formalism neglects internal reflections in the LC layer and is thus only an approximation, although a sufficiently good one, to the exact solution which could be found by Berremans 4×4 formalism. The elements of the resulting matrix \bar{P} (Eq. 1) give the ratios of input vs. output electric field vectors $E_x^{(in)}$, $E_y^{(in)}$, $E_x^{(out)}$, $E_y^{(out)}$. The ratios of transmitted vs. incident intensities are $|P_{ij}|^2$ for the four different combinations of input and output polarization, and

$$I = \sum_{i,j=1}^2 |P_{ij}|^2$$

is the total transmission coefficient of unpolarized light.

If the director twist deformation $\phi(z)$ in the sample is known, the relation between director field and optical transmission is calculated straightforward. Under the assumption that the director deformation is a pure twist ground mode, $\vec{n} = (\cos(\phi(z)), \sin(\phi(z)), 0)$ with $\phi(z) = \phi_m \cos(z\pi/d)$, the transmission intensity as a function of the maximum twist angle (in the middle of the cell) is shown in Fig. 2. A cell thickness of $50.5\mu\text{m}$ and optical parameters of *Mischung 5* have been assumed, the results are shown for three different optical wavelengths. The transmission intensity changes quite linearly with the maximum twist angle when the twist deformation is small, and the curve is antisymmetric with respect to $\phi_m = 0$. Left-handed or right-handed twist lead to opposite changes in the optical transmission. Strictly, the calculations are correct for an in-plane uniform sample, but when the twist domains are large compared to the optical wavelengths, refraction can be neglected and the results remain valid. Oppositely twisted domains appear in the optical pattern as regions of different brightness, a contrast modulation in the transmission texture is expected. In the experiment, comparison of absolute intensities is quite difficult. Therefore we define the contrast $C = 2(I_+ - I_-)/(I_+ + I_-)$ from the difference of the transmission intensity

extrema I_+, I_- of oppositely twisted domains in a sample with periodic twist modulations. This optical contrast is linearly related to the twist amplitude at least for small twist ($< 45^\circ$). Of course, at high twist angles the relation between ϕ_m and the transmitted intensity is no longer linear. The director twist deformation along z will no longer be sinusoidal, other model director fields have to be assumed. Therefore, we restrict the quantitative comparison to voltages near the onset of the chevron texture.

The calculations above have been performed for three different wavelengths only, and the transmission appears to be strongly wavelength dependent. Fig. 4 shows the linear slope of the transmission curve (C/ϕ_m in the vicinity of $\phi_m = 0$) calculated numerically for the complete optical wavelengths band. It shows that knowledge of the wavelength (actually the wavelength / cell thickness ratio) is critical when one is interested in quantitative results. When the sample is illuminated with white light and observed with a B/W camera as in our experiments, it is a sound approximation to use an average slope of 0.0027/deg for the C vs. ϕ_m ratio to establish an approximate quantitative relation between the twist deformation in the sample and measured optical contrast.

Fig. 3 shows the optical transmission as a function of director twist when no phase plate is present (the conventional setup of Fig. 1a). The function is now symmetric with respect to positive and negative twist and the optical contrast is considerably smaller. Only at very high twist deformations, one obtains a substantial optical modulation, but now between non-twisted ($\phi_m = 0$) and twisted regions, that is with $1/2$ wavelength of the twist pattern. Two other arrangements of the polarizers can be described easily. If the analyzer in 1b is rotated to 90° , the optical transmission is complementary to that in Figs. 2 and 3. If the polarizer is turned parallel to the director easy axis, the short wavelength modulation due to the periodic tilt deformation (dielectric convection rolls) will be effective from the beginning and overlaps the interference effect (see experiments).

The more the director field is twisted, the larger is the contribution of the extraordinary wave to the transmission image in the geometry 1b. In that case, the periodic tilt deformation and the diffraction effects of the convection rolls come into play again.

EXPERIMENTAL RESULTS

Figs. 5-7 present a collection of transmission textures under different experimental conditions. All voltages given are scaled with the threshold voltage $U_c = 67.4V$ of the onset of dielectric rolls to the reduced quantity $r = U/U_c$. Fig. 5 shows the first instability above threshold, normal dielectric rolls, observed in standard geometry 1a. Figs. 6,7 depict the development of the chevron pattern at $r = 1.159$ and $r = 1.605$, respectively. The first image (a) is observed with setup 1a, the second (b) shows the texture with a quarterwave plate inserted at 45° , the third (c) corresponds to the setup in Fig. 1b and the last image (d) is the texture under crossed polarizers without phase plate. The director field in normal dielectric rolls (Fig. 5) at $r = 1.005$ is planar in (x, z) , therefore the images in other geometries than setup 1a are trivial and have not been shown there.

Fig. 6, shows a chevron texture at small voltages where the periodic twist deflection already leads to transmission intensity modulations when the phase plate is inserted (6b). The oppositely twisted domains are visible, in particular in the ordinary light where the roll pattern disappears (6c). However, a completely uniform dark image is retained under crossed polarizers when the phase plate is removed (6d). The director twist is too weak to produce substantial contrast between twisted and non-twisted regions.

The comparison of the twist structure visualized in images (b,c) with the corresponding convective rolls pattern (a,b) shows exact agreement of the spatial twist angle modulation and roll pattern. It has to be mentioned also that the director and wave vector modulation have the same phase, i.e. the director is deflected clockwise where the wave vector is deflected clockwise and vice versa.

Fig. 7 presents a chevron texture at high fields where the contrast modulation in geometry 1b is considerable. Even with crossed polarizers and no phase plate, a texture modulation between non-twisted and strongly twisted regions is seen (7d). (Note, however that the contrast of the image presented in Fig. 7d has been enhanced very much.) Fig. 8 visualizes a cross section of the intensity taken normal to the chevrons. The upper curves correspond

to Figs. 6c (solid line) and 7c (dashed) resp., they give the intensity modulation with setup 1b (linear effect). One acknowledges that the spatial modulation is approximately sinusoidal and the modulation amplitude increases with r . The lower curves correspond to profiles under crossed polarizers (quadratic effect). The observed modulation wavelength is half that of the linear effect, the amplitude is much weaker, therefore this effect is only detectable at high r .

A more quantitative analysis is presented in Figs. 9-11. The wavelength of the convection rolls is shown in Fig. 9. It has been extracted from the 2D Fourier transforms of the chevron textures. The wavevectors of the rolls change their orientations away from the x axis with increasing voltages, but their absolute value (wavenumber) is almost unchanged over the whole voltage range. Fig. 10 shows the angles between $\vec{n}_0 \parallel x$ and the wave vectors of the rolls (maximum angles in the middle of the chevron stripes), obtained also by Fourier transform of the images. The transition from normal to inclined rolls is clearly indicated [23]. Left-handed and right-handed domains appear nearly symmetrically. Fig. 11 depicts the corresponding contrast C between the brightness I_+ and I_- , resp., of oppositely twisted domains. The increase in contrast ratio is an empirical measure of the increasing director twist with higher voltage. The exact relation between the twist angle and contrast, however, is quite complex as has been shown in Figs. 2 and 4. When we assume a simple $\phi(z) = \phi_m \cos(z)$ dependence of the twist angle in the cell and an approximately linear relation between contrast and maximum twist ϕ_m with the factor 0.0027/deg derived in the previous section, we can estimate the twist angle modulations. The corresponding scale is shown at the right of Fig. 11. We note, however, that this linear relation bases upon the simulation for small twist angles (see above). The higher contrast measured at high electric fields can be related to the twist angle only qualitatively. The figure shows that the optical contrast and correspondingly the director twist follow roughly the characteristics of the inclination angle of the wave vector.

Finally, we investigate the evolution of the texture after the electric field has been switched off. The relaxation behaviour will help us to extract information on the elastic modes

involved in the z -profile of the twist deformation. Fig. 12a depicts a spatio-temporal image taken with a line scan CCD device. Each horizontal line represents the transmission profile in a cross section taken along the director easy axis \vec{n}_0 , the vertical axis gives the time coordinate t running from top to bottom.

The image 12a was taken with polarizers along x and a phase plate, the observed refraction pattern due to the modulated director tilt in the convective rolls and the long-range twist pattern are superimposed. One can see that while the electric AC field is effective the pattern is strongly modulated in time because the director tilt oscillates with the AC frequency. In addition, one can see five spatial periods of the long-wavelength tilt modulation which correspond to a cut normal to the chevron superstructure (as in Fig. 8, upper curves). After the field is switched off, the tilt modulation decays immediately, within several milliseconds. The moment the electric field was switched off is clearly indicated in the image by the abrupt stop of the high-frequency modulations, the decay time is shorter than the temporal resolution chosen here. This was expected as the driving flow field breaks down instantaneously, and the short wavelength roll pattern is rapidly destroyed by elastic restoring forces. On the other hand, the twist modulation persists for a long time of several seconds after the field has been switched off. The elastic forces which destroy the long wavelength twist pattern are much smaller than those effective in the destruction of the short wavelength convection roll texture. The corresponding decay times are therefore much larger. Fig. 12b shows the decay of the amplitude of the long-wavelength modulation seen in Fig. 12a. We have depicted the absolute value of the respective coefficient in the Fourier transform. The solid line is a fit to a purely monoexponential decay with decay time $\tau = 2.5s$. A rough theoretical estimate of the expected relaxation time for a ground mode sine deformation in z can be obtained from the elastic twist and bend terms involved and the rotational viscosity γ_1

$$\tau \approx \gamma_1 (K_{22}q_z^2 + K_{33}q_x^2)^{-1}$$

with $q_z = \pi/50\mu m$, $q_x = 2\pi/60\mu m$ and the viscoelastic parameters $\gamma_1 = 0.36Pas$, $K_{33} = 13.8pN$, $K_{22} = 6.0pN$ taken from independent magneto-optic measurements of the dynamic

and static Fréedericks transitions, the calculated decay time is 2.1s. In view of the rough approximations used in this calculation, this is in quite reasonable agreement with the experimental decay rate.

DISCUSSION AND SUMMARY

We have shown that the optical investigation of chevron patterns with different microscopic techniques reveals new details of the director field in dielectric dissipative convection structures.

At voltages slightly above the onset of dielectric rolls, we observe stationary normal rolls. The relation between optical texture and director field in these rolls has been shown in a previous paper [22]. At increasing voltage, the director field twists slightly out of the (x, z) tilt plane, accompanied by a corresponding rotation of the wave vector of the rolls out of the x axis direction. Both processes set in at approximately the same critical voltage. The director twist and wave vector modulation follow roughly the same characteristics when the voltage is increased, and both deflections are in phase, such that the structures roughly remain normal rolls on the local scale. The absolute angle of the wave vector modulation can be extracted from the transmission image. The exact director twist angle was estimated from a comparison of the experimental optical images with numerical calculations of the transmission intensity.

The dynamics of the tilt and twist deformations are quite different. As the wavelength of the twist structure is large compared to that of the convection rolls (it corresponds to the periodicity of the chevrons), its elastic restoring forces are very weak, and the twist mode relaxes very slowly. The twist modulation is therefore approximately constant during the cycles of the driving field. This was established in time resolved measurements by means of a fast line scan camera. The tilt modulation of the director in the convection rolls is dynamically fast. It alternates its sign during the cycles of the driving field. This well known theoretical result was confirmed in a previous experiment [22].

From the nearly monoexponential decay of the twist deformation after the driving field is switched off (Figs. 12a,b), we conclude that the z -deformation is basically restricted to the sine ground mode $\propto \sin \pi z/d$ at least near the onset of chevron formation. Higher twist deformation modes should decay much faster and the total decay curve should be non-exponential when more than the ground mode contribute to the z -profile substantially. In summary, the experiments provide information on the relation between director and wave vector structures in chevrons observed in a planar cell. In the theoretical paper by Rossberg [1], simulations showed that the chevron formation is a consequence of the interactions between the in-plane director twist and wave vector fields. It has been argued that this mechanism is general for systems with weakly broken isotropic symmetry, but is quite difficult to verify in planar nematic cells. Our experimental setup provides exactly this test. The results presented are in accordance with the qualitative predictions by Rossberg [1] obtained from the simulations.

In the conduction regime, director twist modulations are observed as well when the driving electric field is sufficiently above the threshold field for conductive rolls. We find that these twist modulations set in approximately at the same field strengths where the stationary normal or oblique rolls start to fluctuate. The study of this effect in the conduction regime may contribute to the understanding of the mechanisms leading to abnormal and fluctuating rolls and will be an interesting future task.

The authors are very indebted to L. Kramer for many useful hints and critical discussions. This study was supported by the DFG with grant STA 425/3-1.

REFERENCES

- [1] A. G. Rossberg, L. Kramer, submitted to *Physica D* (1996).
- [2] L. Kramer, and W. Pesch, *Annu. Rev. Fluid Mech.* **17** 515 (1995). L. Kramer, and W. Pesch, *Electrohydrodynamic Instabilities in Nematic Liquid Crystals* in "Pattern formation in Liq. Cryst." ed. A. Buka and L. Kramer, Springer, NY.
- [3] A. Lindner, privat communication
- [4] A. G. Rossberg, A. Hertrich, L. Kramer, and W. Pesch, *Phys. rev. Lett.* **76** 4729 (1996).
- [5] S. Rasenat; Dissertation, Bayreuth 1990.
- [6] L. K. Vistin, A. Yu. Kabaenkov, S. S. Yakovenko; *Sov. Phys. - Crystallogr.* **26** 70 (1981).
- [7] K. Kondo, A. Fukuda, E. Kuze; *Jpn. J. Appl. Phys.* **20** 1779 (1981). K. Kondo, A. Fukuda, E. Kuze, M. Arakawa; *Jpn. J. Appl. Phys.* **22** 394 (1983).
- [8] H. Richter, S. Rasenat, I. Rehberg; *Mol. Cryst. Liq. Cryst.* **222** 219 (1992).
- [9] V. S. Mylnikov; *Opt. Spectrosc.* **56** 177 (1984).
- [10] S. Rasenat, G. Hartung, B. L. Winkler, I. Rehberg; *Exp. Fluids* **7** 412 (1989).
- [11] Ch. Mauguin; *Bull. Soc. Fr. Mineral. Cristallogr.* **34** (1909).
- [12] P. E. Cladis; *Phys. Rev. Lett.* **28** 1629 (1972).
- [13] P. R. Gerber, M. Schadt; *Z. Naturforsch.* **35A** 1036 (1980).
- [14] T. J. Scheffer and J. Nehring; *J. Appl. Phys.* **56** 908 (1984).
- [15] S. Teitler, and B. W. Henvis; *J. Opt. Soc. Am.* **60** 830 (1970).
- [16] D. W. Berreman, and T. J. Scheffer; *Phys. Rev. Lett.* **25** 577 (1970). D. W. Berreman, *J. Opt. Soc. Am.* **62** , 502 (1972).
- [17] R. C. Jones; *J. Opt. Soc. Am.* **31** 488 (1941), **38** 671 (1948).

- [18] P. Yeh; *J. Opt. Soc. Am.* **72** 507 (1982). P. Allia, C. Oldano, and L. Trossi; *J. Opt. Soc. Am.* **B 5** 2452 (1988). D. J. DeSmet; *Surf. Sci.* **217** 413 (1989). H. L. Ong; *J. Opt. Soc. Am.* **A 10** 283 (1993). H. L. Ong; *Jpn. J. Appl. Phys. Pt. 2* **30** L1028 (1991). C. Gu, P. Yeh; *Applied Optics* **33** 60 (1994).
- [19] see e.g. M. Grigutsch, N. Klöpffer, H. Schmiedel and R. Stannarius; *Mol. Cryst. Liq. Cryst.* **262** 283 (1995).
- [20] U. Schuhmacher, *Dissertation* Halle 1987.
- [21] H. Amm, *Diplomarbeit* Leipzig 1997.
- [22] R. Stannarius, M. Grigutsch, and H. Amm; *J. Physique* (submitted 1996).
- [23] We do not use the term oblique rolls here because the director still seems to be rather normal to the convection rolls.

FIGURES

FIG. 1. Experimental geometry of the cell, polarizers and $\lambda/4$ plate. The rubbing direction is x , z is normal to the cell plane. (a) setup for the observation of the director tilt profile (b) setup sensitive to the director twist profile. (c) Schematic presentation of the cell with the convection rolls in the chevron texture (top) and the corresponding director twist in the sample (bottom).

FIG. 2. Calculated optical transmission for the setup in Fig. 1b, with $d = 50.5\mu m$, $n_e = 1.6315$, $n_o = 1.4935$, and a sine dependence of the director twist $\phi(z) = \phi_m \sin \pi z/d$. The wavelengths are 500nm (—), 550nm (- - -) and 600nm (. . .). Transmission is normalized to the total incident light passing the polarizer.

FIG. 3. Same as in Fig. 2 but with setup of Fig. 1a. Note the change in the vertical scale.

FIG. 4. Calculated linear slope of the contrast C vs. ϕ_m (per degree) for wavelengths in the optical spectrum, sample parameters as in Fig. 2.

FIG. 5. Transmission texture ($200\mu m \times 200\mu m$) of the normal dielectric rolls of *Mischung 5* at $U=67.7V$ ($r = U/U_c = 1.005$). Sample parameters $d=50.5\mu m$, $f = 50Hz$, $T = 30^\circ$, $U_c = 67.4V$.

FIG. 6. Transmission textures ($200\mu m \times 200\mu m$) of chevrons (at $r = 1.159$) under different orientations of the polarizers and quarterwave plate, sample parameters as in Fig. 5. (a) conventional technique (polarizers along x). (b) quarterwave plate inserted at 45° orientation, one sees the convection rolls and the superimposed twist effect, (c) polarizer in 90° orientation to x . Now, only the twist pattern remains visible, the tilt pattern is no longer observed, the intensity modulation is complementary, (d) crossed polarizers, no modulation is seen.

FIG. 7. Images as in Fig. 6 for $r = 1.604$. At this field strength, the intensity modulation between non-twisted and twisted regions becomes visible even under crossed polarizers when the contrast is sufficiently enhanced by digital processing (d).

FIG. 8. Upper curves: Intensity cross sections of images 6c (solid) and 7c (dashed). The modulation corresponds to the chevrons period. For comparison, the lower curves show the corresponding cross sections of images 6d (solid) and 7d (dashed). A contrast modulation with half wavelength is indicated in the high voltage texture but not visible in the low voltage texture.

FIG. 9. Experimentally determined wavelength of the convection rolls in the chevron texture in dependence upon the reduced driving voltage. λ_0 gives the periodicity of the optical image which is half the wavelength of the director tilt pattern (sample parameters as in Fig. 5).

FIG. 10. The angle θ between the wave vector of the convection rolls and the director easy axis as a function of the reduced voltage (sample parameters as in Fig. 5). The two branches correspond to the oppositely inclined chevron domains.

FIG. 11. Experimentally determined optical contrast C between regions of maximum and minimum transmission intensity (opposite director twist) as a function of the reduced voltage (sample parameters as in Fig. 5). Note linear scale given at the right hand side is reliable only to approximately 45° , see text.

FIG. 12. a) Evolution of the optical pattern after the electric field is switched off from $r = 1.162$. The horizontal axis represents a cross section of the transmission image along the director easy axis, the vertical coordinate is the time axis (1.6s). The moment the field is switched off is clearly marked by the end of the fast temporal oscillations, the slow decay of the twist deformation is visible. b) Time dependence of the twist modulation amplitude calculated from the spatial Fourier transforms. The solid line is a fit to an exponential decay with time constant 2.5s.

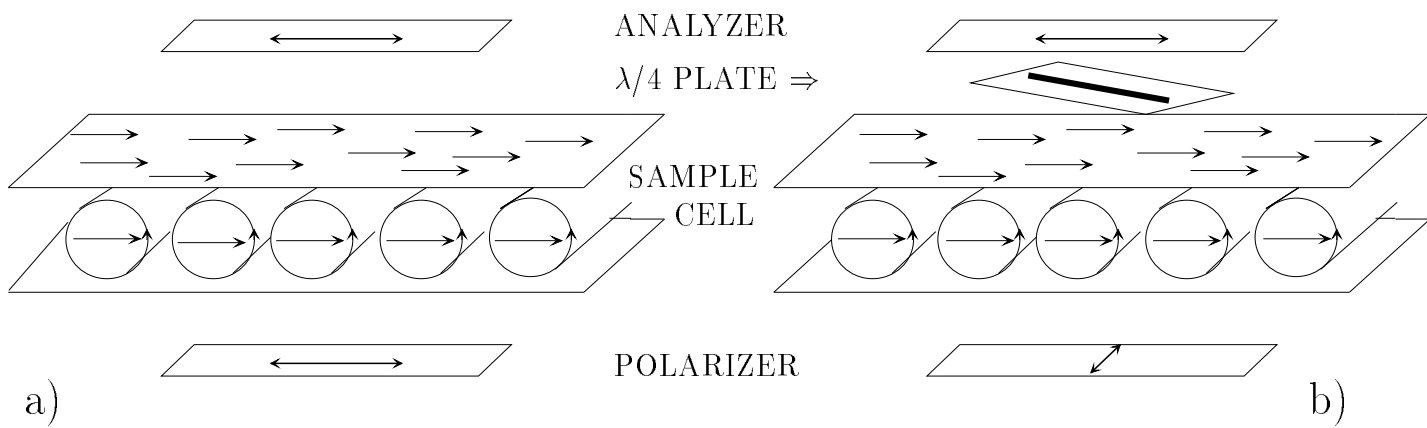


Fig. 1a,b

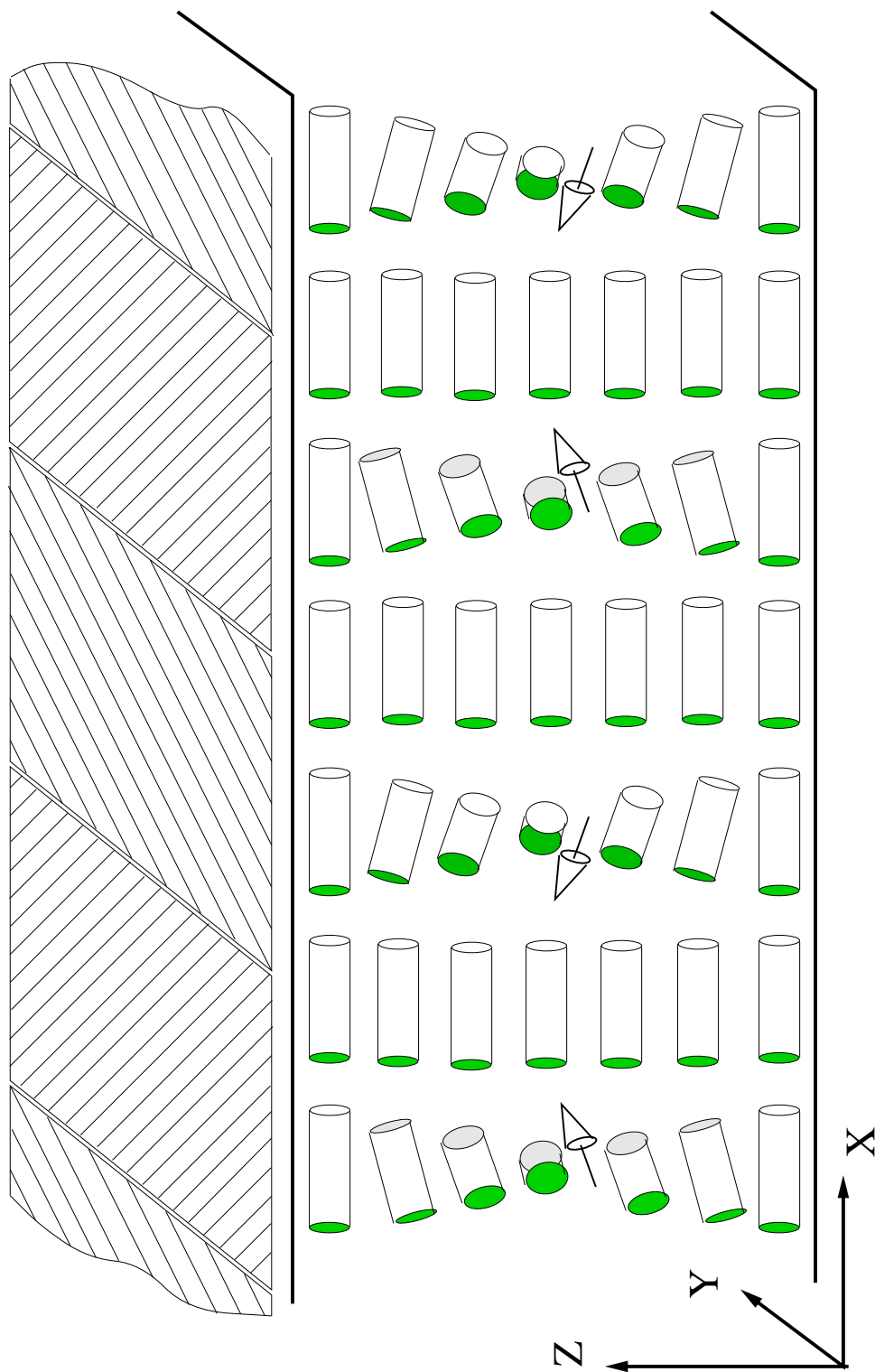


Fig. 1c

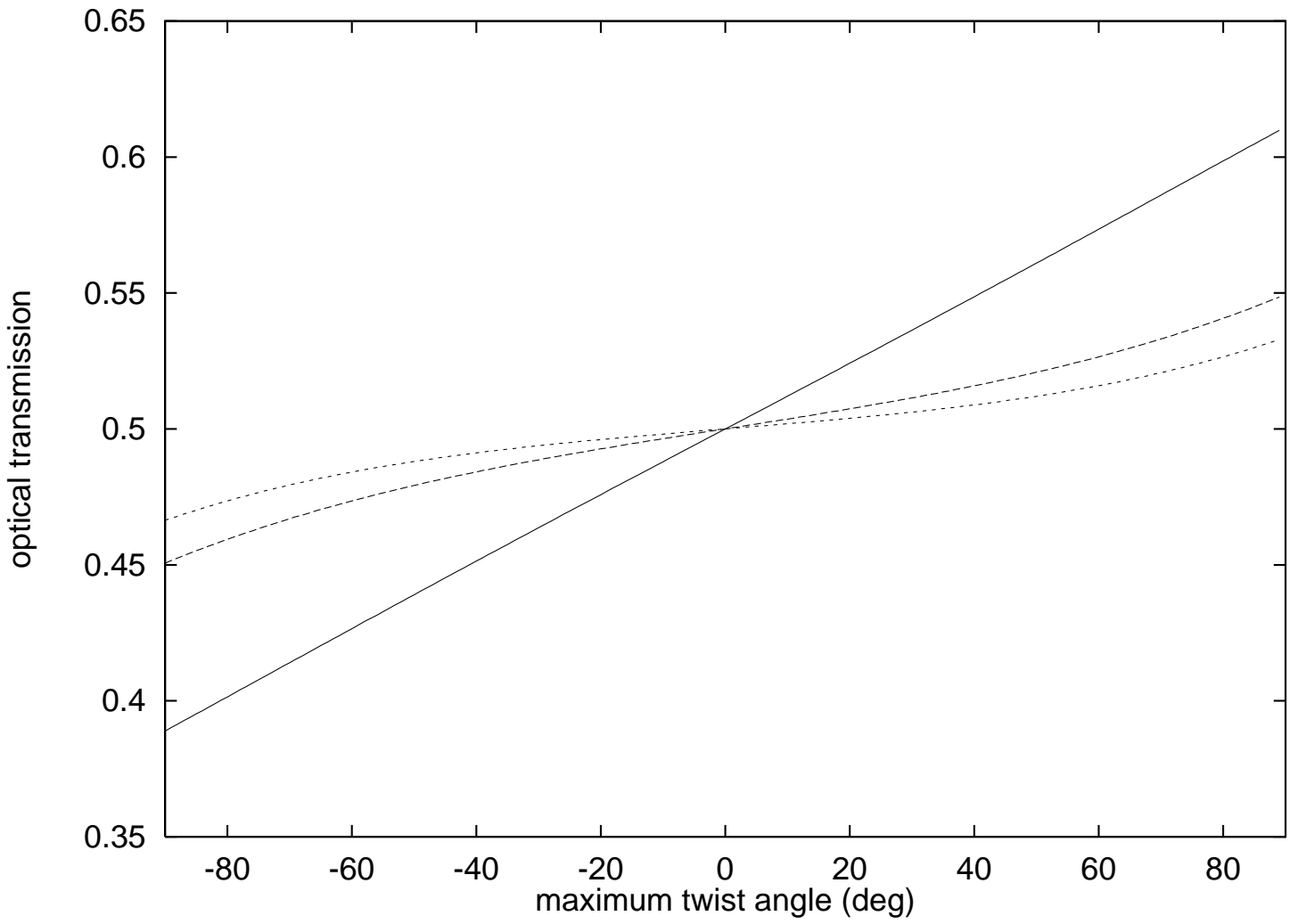


Fig. 2

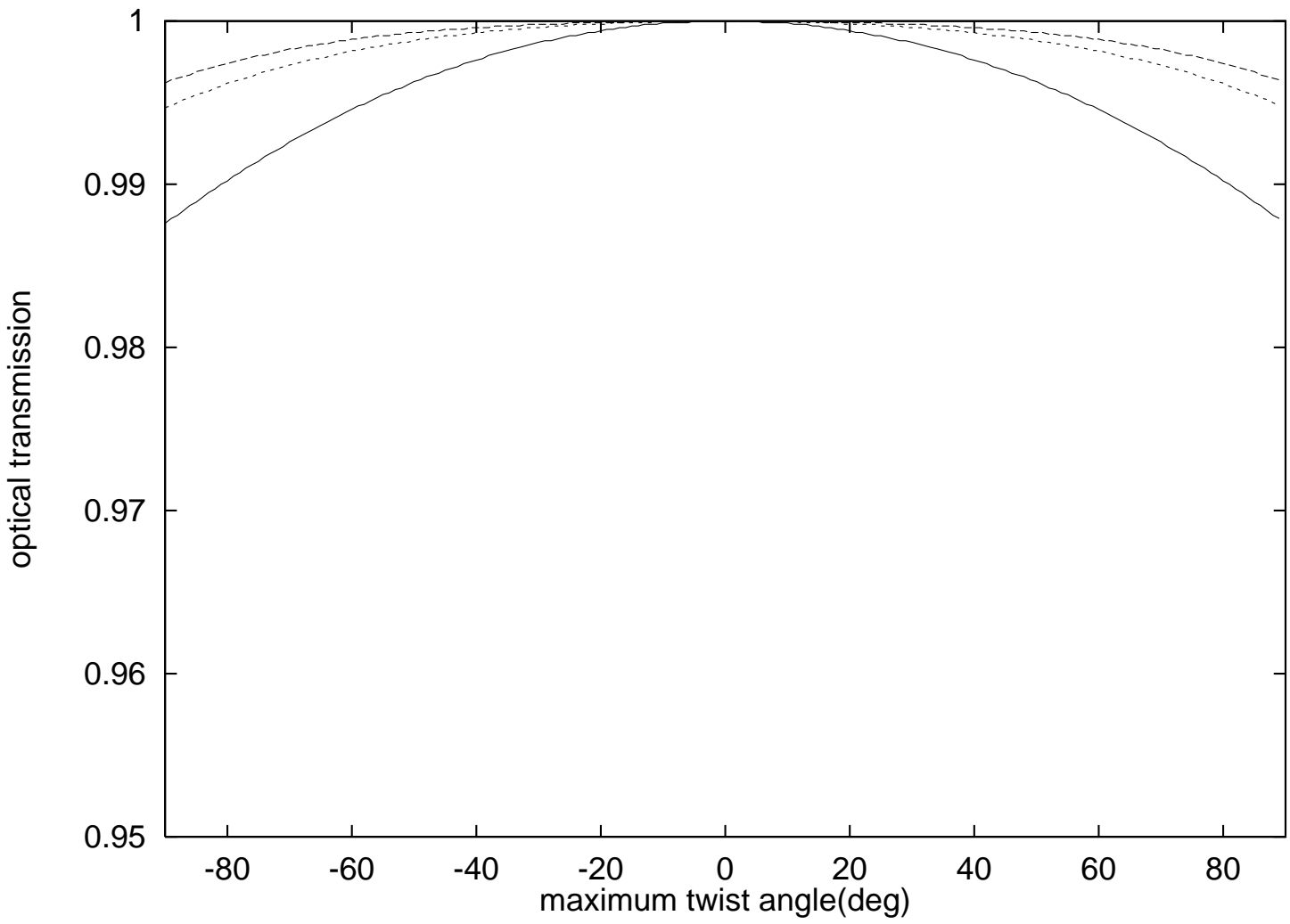


Fig. 3

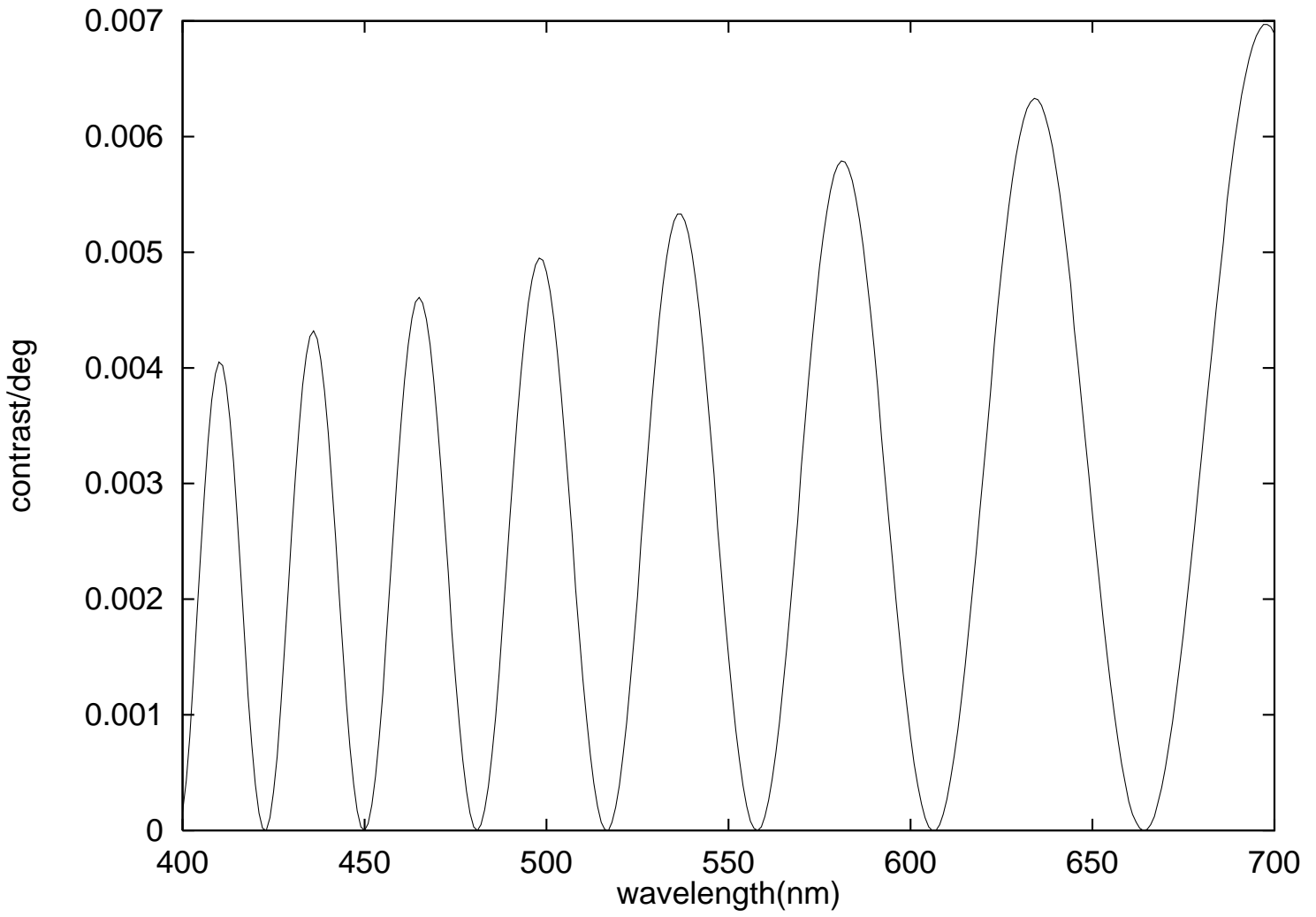


Fig. 4

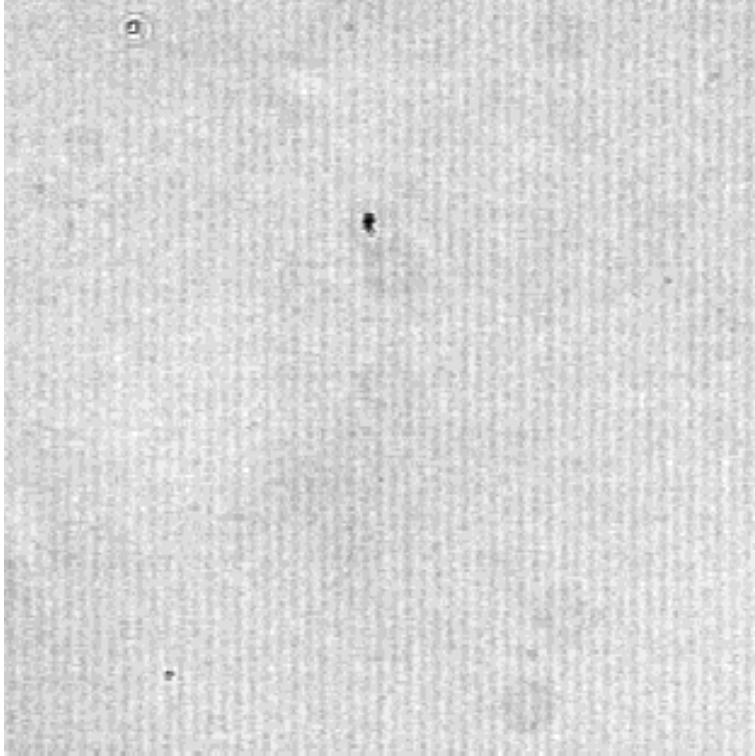


Fig. 5

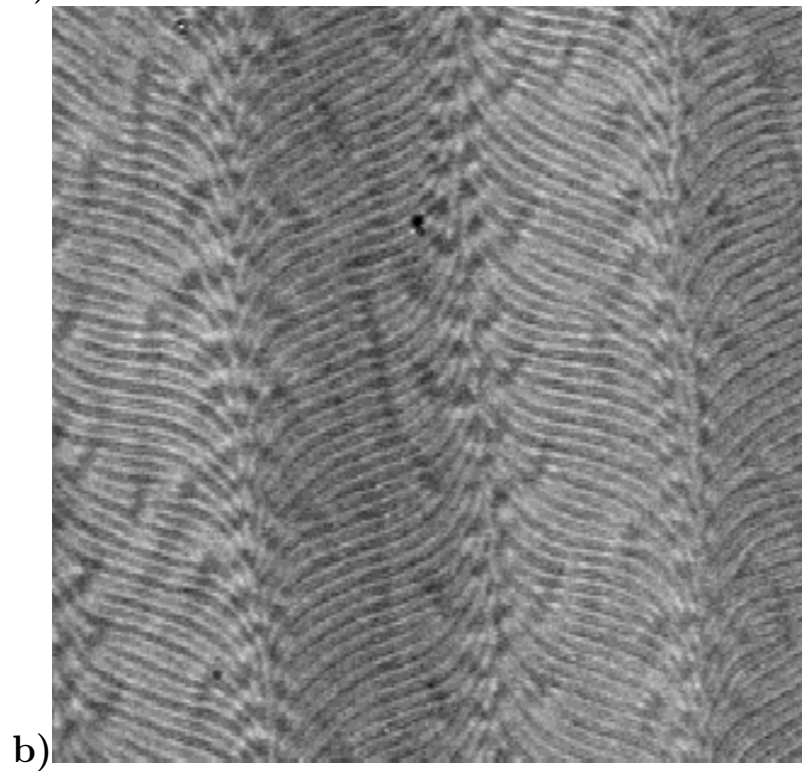
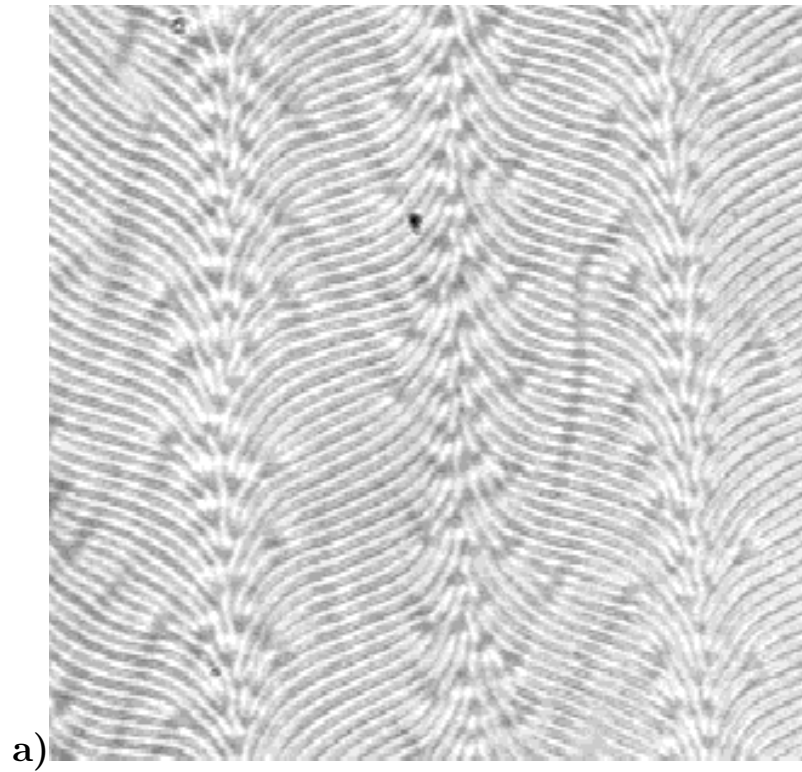
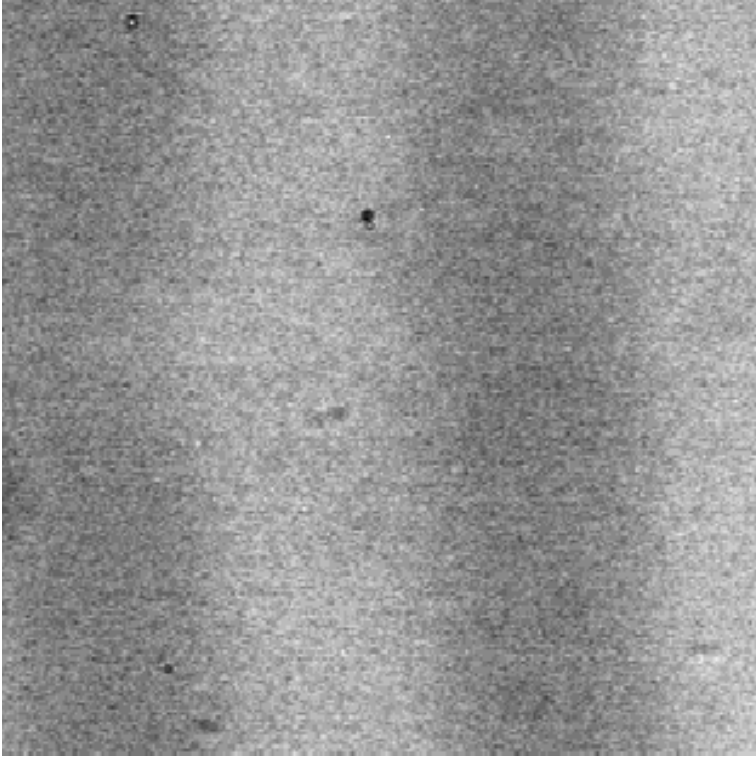
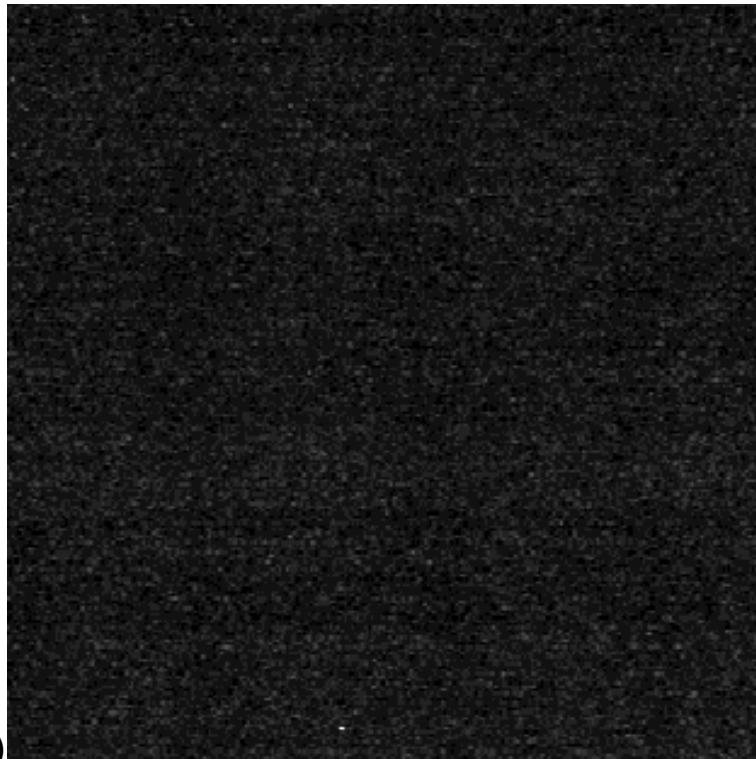


Fig. 6



c)



d)

Fig. 6

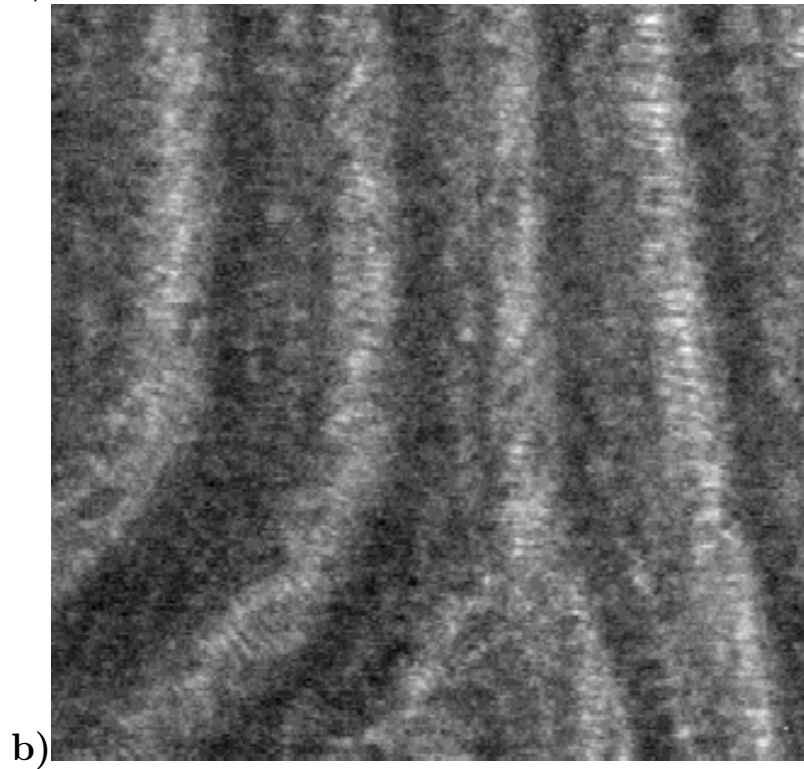
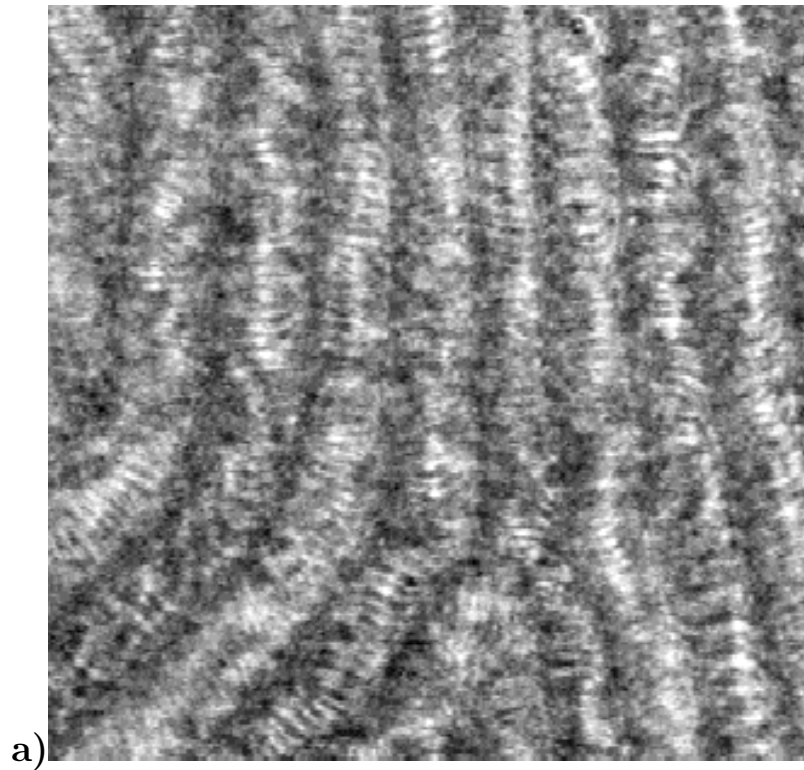
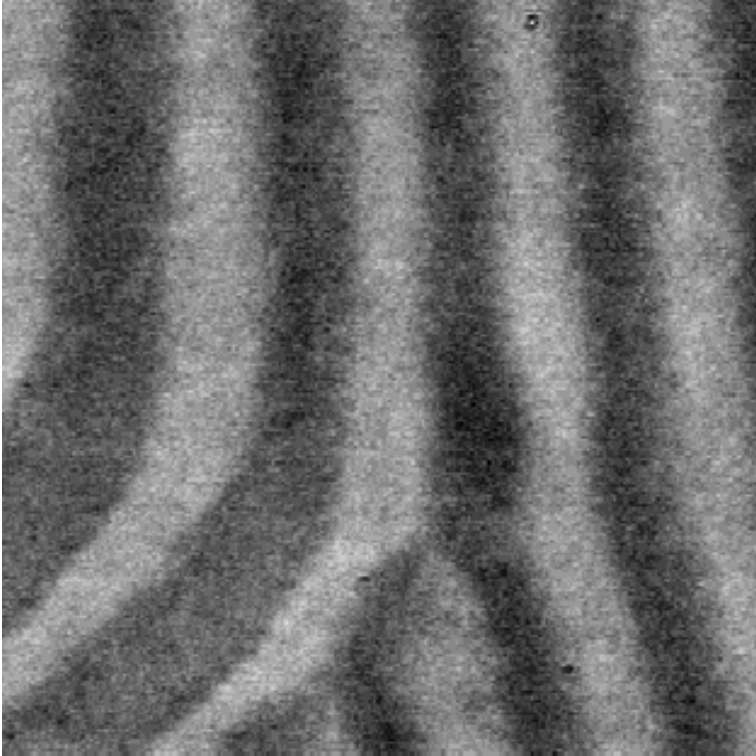
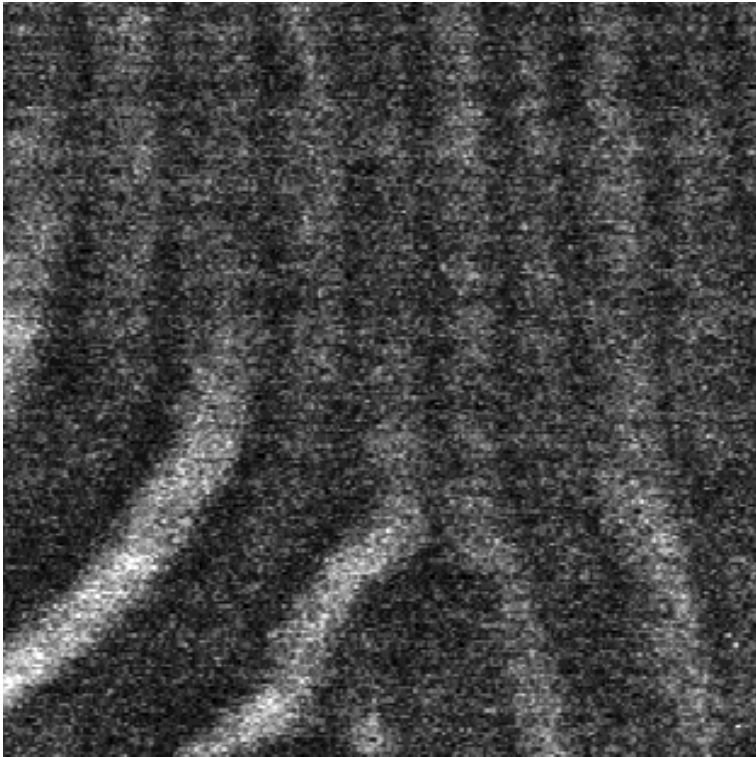


Fig. 6



c)



d)

Fig. 7

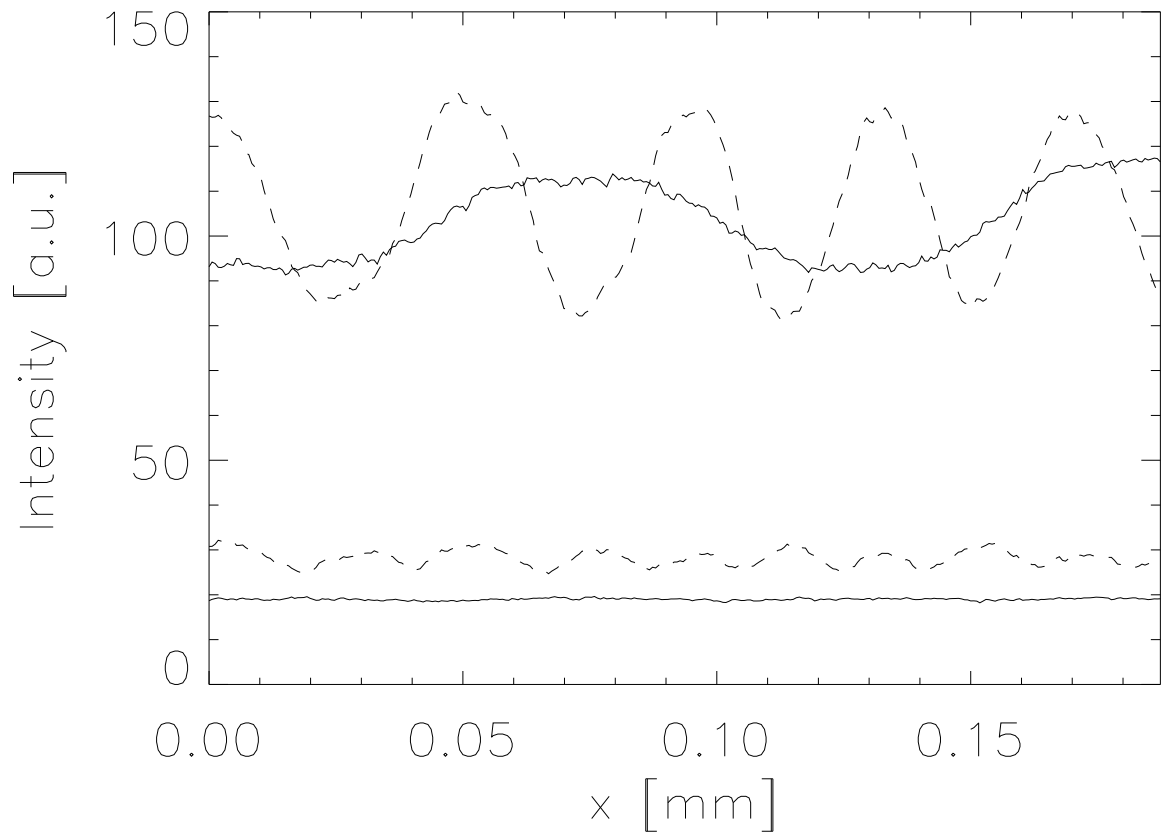


Fig. 8

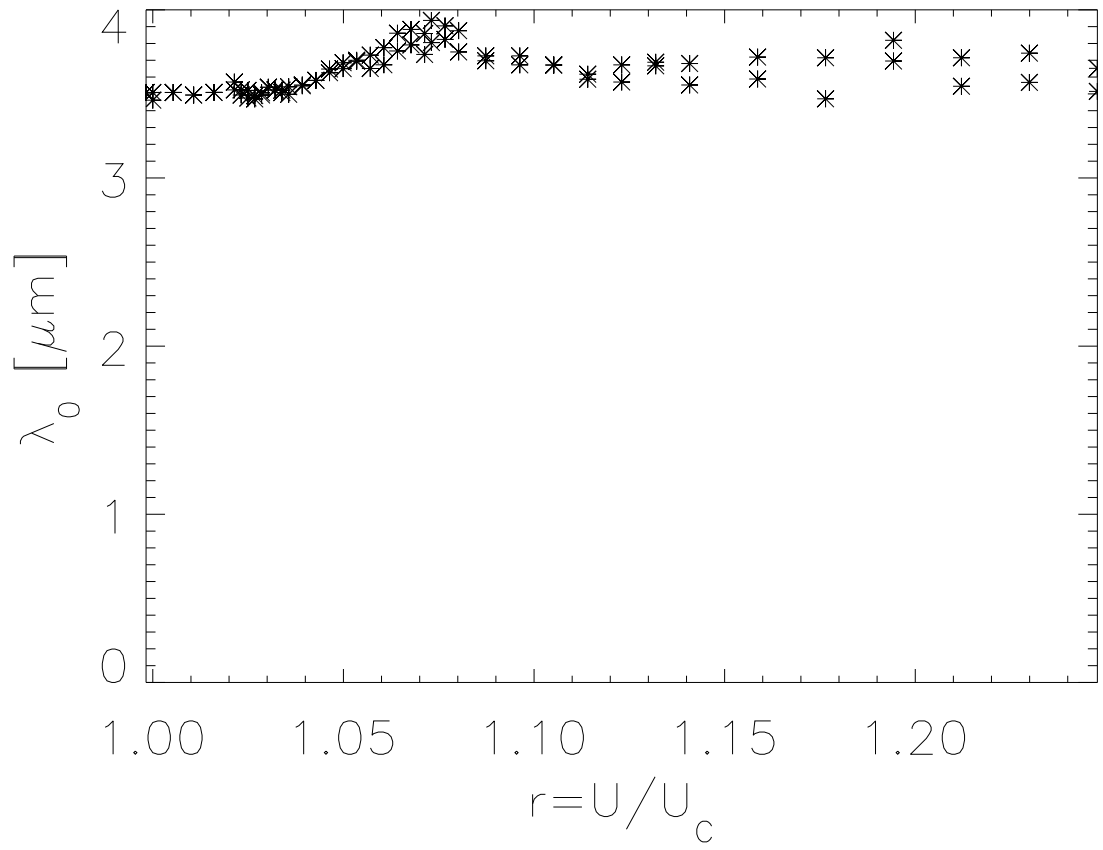


Fig. 9

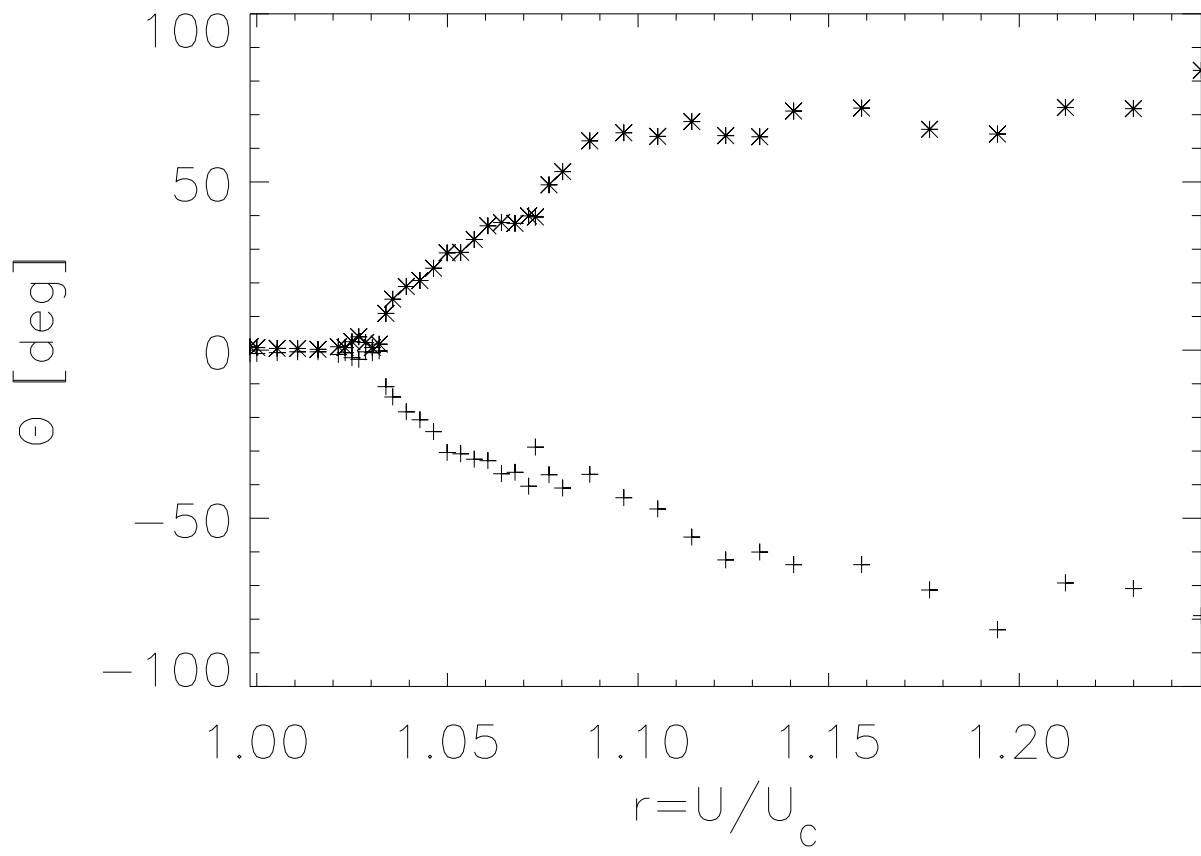


Fig. 10

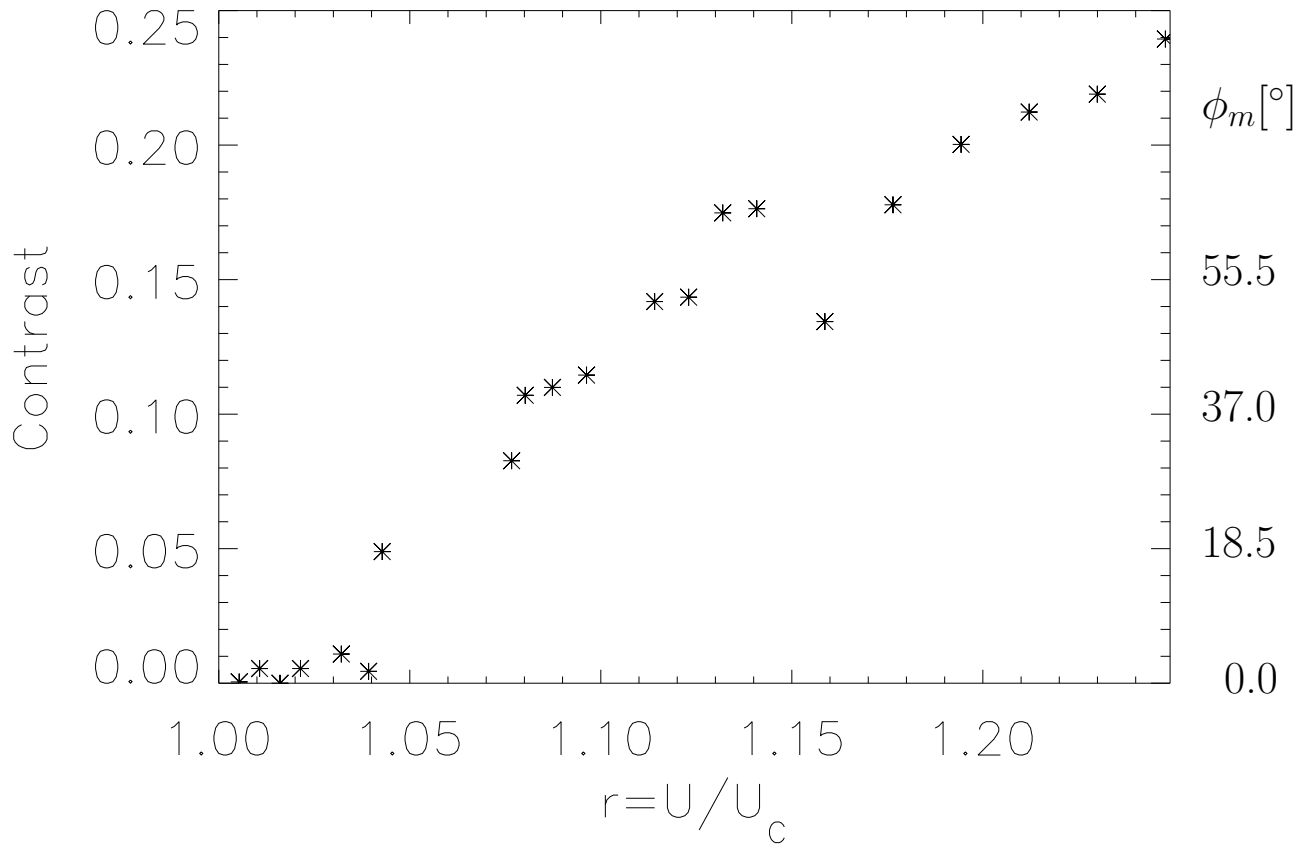
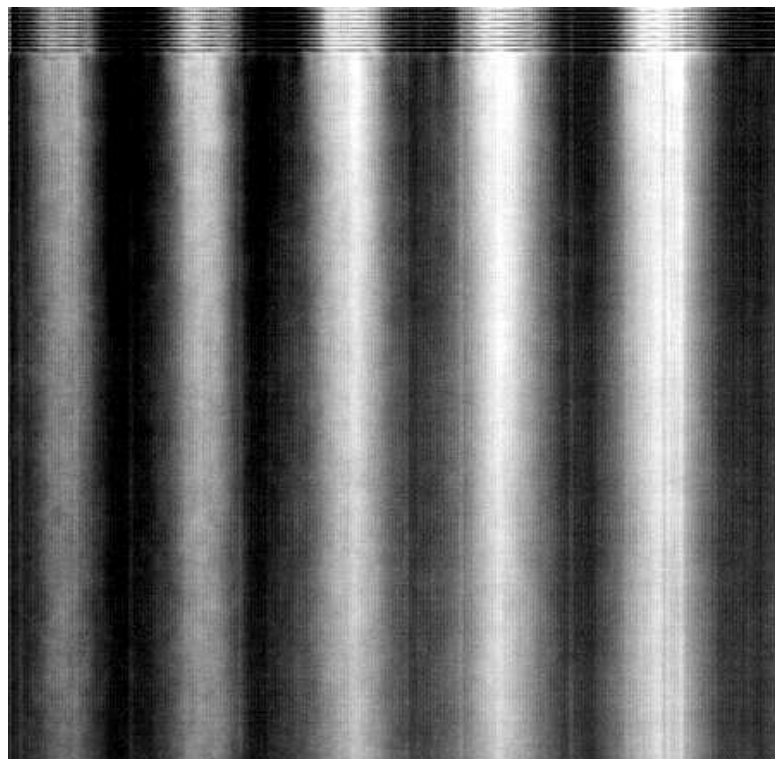
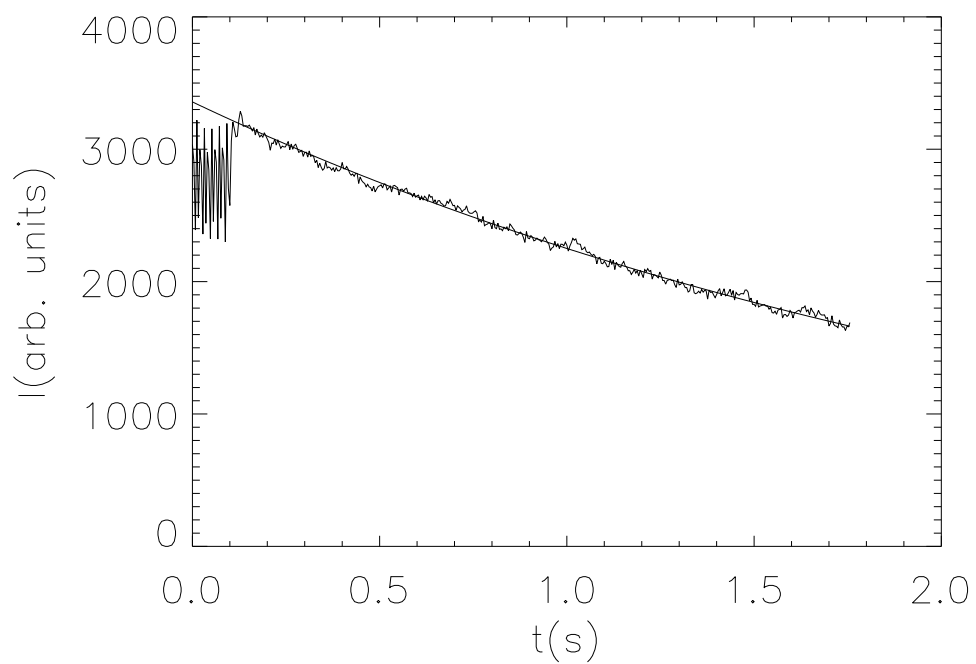


Fig. 11



a)



b)

Fig. 12